Detection of critical PM$_{2.5}$ emission sources and their contributions to a heavy haze episode in Beijing, China, using an adjoint model

Shixian Zhai[1], Xingqin An[2], Tianliang Zhao[1], Zhaobin Sun[3,4], Qing Hou[2], Chao Wang[2]

[1]Key Laboratory for Aerosol-Cloud-Precipitation of China Meteorological Administration, Collaborative Innovation Center on Forecast and Evaluation of Meteorological Disasters, School of Atmospheric Physics, Nanjing University of Information Science & Technology, Nanjing 210044, China

[2]State Key Laboratory of Severe Weather, Key Laboratory of Atmospheric Chemistry of CMA, Chinese Academy of Meteorological Sciences, Beijing 100081, China

[3]Institute of Urban Meteorology, China Meteorological Administration, Beijing 100089, China

[4]Environmental Meteorology Forecast Center of Beijing-Tianjin-Hebei, China Meteorological Administration, Beijing, 100089, China

Correspondence to: Xingqin An (anxq@camscma.cn) and Tianliang Zhao (tlzhao@nuist.edu.cn)

Abstract. Air pollutant sources and regional transport are important issues in air quality control. The Global–Regional Assimilation and Prediction System coupled with CMA Unified Atmospheric Chemistry Environment (GRAPES–CUACE) aerosol adjoint model was applied to detect the sensitive emission sources of a haze episode in Beijing during 19–21 November 2012. High PM$_{2.5}$ concentration peaks occurred at 05:00 and 23:00 LT (GMT+8) over Beijing municipality on 21 November 2012, which were set as the objective functions for the aerosol adjoint model. The sensitive emission regions of the first PM$_{2.5}$ peak were tracked to the west and south of Beijing with 2- to 3-day cumulative transport of air pollutants to Beijing, whereas the sensitive emission regions of the second peak were mainly located to the south of Beijing, where southeasterly moist air transport led to the hygroscopic growth of particles and pollutant convergence in front of the Taihang Mountains in the daytime of 21 November The temporal variations of the sensitivity coefficients for the two PM$_{2.5}$ concentration peaks reveal that the response time of Beijing haze pollution to local emissions is about 1–2 hours, and that to the surrounding emissions is about 7–12 hours. The upstream Hebei province has the largest impacts on the two PM$_{2.5}$ concentration peaks, and the contribution of Hebei emissions to the first PM$_{2.5}$ concentration peak (43.6%) is greater than to the second PM$_{2.5}$ concentration peak (41.5%). The second largest emission contributing province is Beijing (31.2%), followed by Shanxi (9.8%), Tianjin (9.8%) and Shandong (5.7%) for the 05:00 PM$_{2.5}$ peak, and Beijing (35.7%) followed by Shanxi (8.1%), Shandong (8.0%) and Tianjin (6.7%) for the 23:00 PM$_{2.5}$ peak. The adjoint results were compared with the forward sensitivity simulations of the Models-3/CMAQ system. The two modelling approaches are highly comparable in their assessments of atmospheric pollution control schemes for critical emission regions, but the adjoint method has higher computational efficiency than the forward sensitivity method. This work also reflects that controlling air pollutant sources from adjoint sensitive emission regions has better effects and higher efficiency than controlling emission sources from emission intensive regions.

1. Introduction

The application of the adjoint theory to atmospheric chemistry models can enable efficient calculation of sensitivities of a few variables or metrics with respect to a large number of input parameters (Marchuk, 1974; Sandu et al., 2005; Hakami et al., 2007). Classic source-oriented atmospheric chemistry models use inputs of emissions to output the spatial-temporal variation of pollutants. By contrast, receptor-oriented adjoint models take the gradients of the objective function to model variables as inputs, and output the spatial-temporal variations of the sensitivity of the objective function to model parameters (Errico, 1997; Carmichael et al., 2008). Therefore, in concentration source sensitivity analysis problems, the calculation efficiency of the adjoint method is much higher than that of the traditional finite difference method, which requires repeated input perturbations and result comparisons (Wang et al., 2015). Moreover, the finite difference approach changes the state of the modelled atmosphere and inevitably incurs truncation and cancellation errors (Constantin and Barrett, 2014). The adjoint model integrates under certain atmospheric conditions while calculating gradients, and thus can provide exact sensitivities. As a result, if we set the objective function as the pollutant concentration over a region at a point in time (or during a time period), the adjoint sensitivity approach can detect sensitive emission sources in detail by revealing the changes in concentration due to perturbations in emission sources.

Beijing is a rapidly growing economic centre and densely populated metropolis, and its recent $PM_{2.5}$ pollution problems have garnered considerable attention (Zhang et al., 2016; Sun et al., 2014; Guo et al., 2010; Wu et al., 2015). $PM_{2.5}$ pollution in Beijing is significantly influenced by regional transport of pollutants from its environs, and joint control of air pollutant emission sources has been promoted. Research using approaches like the flux calculation method (An et al., 2007), the back-trajectory model (Zhai et al., 2016), and the observation analysis (Li et al., 2016) have revealed that southerly wind almost always resulted in high $PM_{2.5}$ conditions in Beijing. Studies have also pointed out that more than 50% of $PM_{2.5}$ pollutants originate in surrounding provinces and cities, including southern Hebei, Tianjin, eastern Shanxi, and Shandong provinces (Jiang et al., 2015; Gao et al., 2016). Studies also show that joint regional air pollution control can be more cost-effective (Wu et al., 2015), and that joint control schemes in sensitive source zones (detected by a back-trajectory model) prior to unfavorable meteorological conditions can help reduce costs and improve efficiency (Zhai et al., 2016). The above studies either provided pollutant pathways through meteorological analysis or analyzed air pollutant concentration sensitivities to a limited group of emission sources. However, if air pollution is spatially and temporally traced back to its emission sources, decision making regarding air pollution can be better addressed.

Differently from back trajectories or statistical factor analysis, the adjoint approach accounts for chemical and physical processes combined with transport, and can efficiently estimate the incremental influence of specific sources on air quality (Henze et al., 2009). Recently, An et al. (2016) developed an adjoint model of GRAPES-CUACE and estimated the

sensitivity of average black carbon (BC) concentrations over Beijing at the highest concentration time with respect to BC amounts emitted over the Beijing-Tianjin-Hebei region and pointed out the effectiveness of controlling the most influential regions during critical time intervals detected by the adjoint sensitivity analysis. Zhang et al. (2015) attributed sources of Beijing $PM_{2.5}$ using the adjoint GEOS-Chem model and summarized that residential (49.8%) and industrial sources (26.5%) make the largest contributions, and that 45%–53% $PM_{2.5}$ pollutants in Beijing and Tianjin are from local sources, whereas Hebei province sources contribute about 26%. Both Zhang et al. (2015) and An et al. (2016) showed the high efficiency and accuracy of atmospheric chemistry adjoint model in Beijing air pollutant source apportionment.

In this study, we apply the newly developed GRAPES–CUACE (Global–Regional Assimilation and Prediction System coupled with CMA Unified Atmospheric Chemistry Environment) aerosol adjoint model (An et al., 2016) to track the sensitive emission sources of a high $PM_{2.5}$ episode in November 2012 Beijing, during which time two $PM_{2.5}$ concentration peaks occur and are set as the objective functions. By detecting sensitive emission sources of these two hourly $PM_{2.5}$ peaks, our work advances the understanding of emission source impacts by providing detailed insights into the spatial and temporal variability of emission source contributions from each of the surrounding provinces as well as from local and environs transports. We then set the average $PM_{2.5}$ concentration on 21 November as the objective function and compared the adjoint results with the Models-3/CMAQ assessments (Zhai et al., 2016). In addition, we also compared emission sources impacts to Beijing $PM_{2.5}$ peak from adjoint sensitive zones and emission intensive zones. This study explores the capability of the GRAPES–CUACE aerosol adjoint model in simulating the concentration–source relationships in detail and provides guidance for flexible environmental control policy.

2.   Synoptic analysis of the pollution episode

Atmospheric stability and humidity over the mid-east region of China from 19 to 22 November 2012 were analysed in combination with Meteorological Information Comprehensive Analysis Processing System (MICAPS) results, the sounding stratification and the dew point-pressure curves (temperature-logarithmic pressure diagrams) at Nanjiao Station in Beijing (Figure 1), and the flow field pattern. Meanwhile, the forming processes of two pollution peaks at dawn and at night on 21 November 2012 are also qualitatively analysed. From 19 to 20 November, Beijing was under the influence of a low-pressure system between two high pressures. During the daytime of 19 and 20 November, southerly winds prevail below 925 h Pa and 1000 h Pa, and the relative humidity increased during this time period. During the night-time periods of 19 and 20 November, southerly winds shifted to northeasterly and easterly winds, which brought pollutants together with water vapour to Beijing. Meanwhile, thermal inversions existed below 850hPa during these two days. The above analysis reveals that $PM_{2.5}$ concentration accumulation was tightly connected with southerly wind during the daytime and the easterly wind at night.

During the daytime on 21 November, the Beijing-Tianjin-Hebei area was at the bottom of a high pressure system, with easterly winds prevailing in the 850hPa layer. The thermal inversion remained, and the relative humidity continued to increase. Mid-south Hebei was influenced by cold air and was controlled by northerly winds, while Beijing was mainly under the influence of an easterly wind that promoted pollutant convergence in front of the Taihang Mountains and carried abundant water vapour which accelerated hygroscopic growth of local particles. It can be concluded that the pollution peak on the night of 21 November is not only the result of pollutant accumulation during the previous 2 days, but also the result of hygroscopic growth of local particles and pollutant convergence caused by the easterly wind during the daytime of 21 November. According to previous research (Chen et al., 2016; Li et al., 2016), this is a typical synoptic episode that gradually generates air pollutants over Beijing until a sudden and significant improvement of air quality results from strong winds. This is also the same episode that is analysed in Zhai et al. (2016), thus facilitating further comparisons.

3. Methods

3.1. Concepts of adjoint sensitivity analysis

Sensitivity analysis plays an important role in atmospheric environment research. Knowledge of the impacts of emission sources on pollutant concentrations can help enact effective air pollution control strategies. The adjoint model is efficient at calculating the sensitivity of an objective function to any model variable at any time step. Figure S2 contains schematic diagrams of the forward atmospheric chemistry model and adjoint model. The atmospheric chemistry model takes emissions (S: $S_1, S_2, \ldots, S_n, \ldots, S_N$) as inputs and outputs pollutant concentrations (C: $C_1, C_2, \ldots, C_m, \ldots, C_M$) through forward integration. Any emission source Sn, might has an influence on the concentration at any receptor site C_m. A pair of emission source sensitivity tests, using the traditional source-oriented finite difference method, can obtain the contribution from one emission source (or a combined group of emission sources) to pollutants at any receptor site. Therefore, with N emission sources and M receptors in total, the pollutant contribution from each of the N emission sources to each of the M receptors (an N×M matrix) can be obtained through N+1 iterations of forward integration (one base simulation included).

The receptor-oriented adjoint model is complementary to the forward model. The sensitivity map of a scalar function of pollutant concentration (the objective function) to every emission source (N×1 matrix) can be obtained through one backward adjoint integration (Sandu, 2005; An et al., 2016; Zhai, 2015), and the above-mentioned N×M matrix requires M iterations of adjoint integration. Theoretically, the resulting N×M matrix from the forward and backward methods are the same within a small perturbation (Marchuk, 1986). Therefore, an atmospheric chemistry model is suitable for simulating air pollution processes, whereas an adjoint model is efficient in quantifying receptor-source relationships. A detailed comparison of the computational costs of forward and adjoint sensitivity analyses can be found in the supplement.

The adjoint model can work out the sensitivity of the objective function J to any emission source Sn, denoted $\partial J/\partial S_n$. If we

125   compare a group of uniformly distributed emission sources, larger $\partial J/\partial S_n$ values indicate greater influence of emission source S_n on J. However, emission intensities are obviously not uniform between urban and rural areas, and seasonal and diurnal changes add even more nonuniformity. In addition, emissions of different species may have different units and may differ in order of magnitude. Under these circumstances, the relative contribution of each emission source cannot be determined only by the gradient $\partial J/\partial Sn$. Therefore, we define the sensitivity coefficients in this study as $(\partial J/\partial S_n)\cdot S_n$, which shares the same unit

130   with the objective function, and reflects the absolute changes in the objective function due to perturbations in emission sources, thus making contrast among emissions sources more convenient.

3.2. Model description

The GRAPES–CUACE is an online coupled atmospheric chemistry modelling system (Wang et al., 2009; Zhou et al., 2012; Jiang et al., 2015) developed by the China Meteorological Administration (CMA). GRAPES-Meso is a regional

135   meteorological model (Xue et al., 2008) within GRAPES–CUACE, and CUACE is an atmospheric chemistry modelling system independent of meteorological and climate models (Gong et al., 2009). The CUACE system adopted the size-segregated multi-component aerosol algorithm CAM (Canadian Aerosol Module) (Gong et al., 2003) as its aerosol module and the second generation of Regional Acid Deposition Model (RADM Ⅱ) mechanism (Stockwell et al., 1990) as its gaseous chemistry. CAM contains numerous major aerosol processes in the atmosphere: generation, hygroscopic growth,

140   coagulation, nucleation, condensation, dry deposition/sedimentation, below-cloud scavenging, aerosol activation and chemical transformation of sulphur species in clear air and in clouds (Gong et al., 2003), which is coherently integrated with the gaseous chemistry in CUACE. Since the nitrates and ammonium formed through the gaseous oxidation are unstable and prone to further decomposition back to their precursors, CUACE adopts ISSOROPIA to calculate the thermodynamic equilibrium between them and their gas precursors (Zhou et al., 2012). The CUACE system is compatible with various kinds of

145   meteorological models and can be used as a common platform for atmospheric constituent calculation.

The GRAPES–CUACE aerosol adjoint model was developed by applying adjoint theory to the GRAPES–CUACE modelling system. It includes the adjoint of CAM (Canadian Aerosol Module, Gong et al., 2003), the adjoint of the three interface programmes that connect GRAPES-Meso and CUACE, and the adjoint of the aerosol transport processes. Therefore, the GRAPES–CUACE aerosol adjoint model is capable of coupling major aerosol processes in the atmosphere into its simulations

150   of the sensitivities of the objective function to primary aerosol sources. Therefore, S_n defined in section 3.1 includes BC, OC, sulphate, nitrate and fugitive dust particles.

Figure S3 shows the operational processes used in this study. In order to ensure that the forward and the backward models were in the same chemical state, the forward GRAPES–CUACE model was first integrated to save the unequilibrated variables (the so-called "state concentrations") in checkpoint files at the beginning of each external time step (Sandu et al., 2005; Henze et al.,

155   2007). These saved variables were then input at each cheque point during the backward adjoint integration. To handle intermediate variables, this study adopted recalculation and stack storage (PUSH & POP) schemes. Details about the construction, framework and operational flowchart of the GRAPES–CUACE aerosol adjoint model are discussed in An et al. (2016).

3.3. Model setup, data and validation

160   The simulated domain in this study covered northeast China (105°E –125°E, 32.25°N –42.25°N) (Figure 4), which included 41×23 simulation grid cells with 31 vertical layers at the resolution of $0.5°\times0.5°$. The model integrated at a time step of 300s. The National Centers for Environmental Prediction (NCEP) Final Analysis (FNL) dataset was used to define the initial meteorological field and the meteorological boundary conditions. The initial and boundary values for O_3 and OH were taken from climatic means and zeros for each aerosol species during the first run, then the daily initial values of all chemical species

165   were determined by the 24-h forecast made by the previous day's simulation. To eliminate the discrepancy between the idealized initial concentration field and the real concentration field, the simulation started at 20:00 Beijing LT (GMT+8) on 10 November 2012 and the analysed period ran from 20:00 LT on 17 November 2012 to 20:00 LT on 22 November 2012.

This study used hourly gridded off-line emission source processed by the SMOKE module, which is based on statistical data from government agencies for 2007 for anthropogenic emissions. Anthropogenic emissions include five aerosol species of

170   black carbon (BC), organic carbon (OC), sulphate, nitrate and fugitive dust particles, in addition to 27 gases, such as VOCs, NH_3, CO, CO_2, SO_x and NO_x (Cao et al., 2011). Emission source types include biomass combustion, residences, power generation, industry, transportation, livestock and poultry breeding, fertilizer use, waste disposal, solvent use, and light industrial product manufacture (Cao et al., 2011). Besides, natural sea salt and natural sand/dust emissions are also calculated in the model.

175   Figure 2 illustrates the gridded distribution of the overall primary particle sources and Fig. 3 shows the hourly variability of the overall particle sources (as well as sulphate as an example) in Beijing. In Fig. 2, four intensive source zones over Beijing and its surrounding provinces: 1) southern Beijing and Tianjin (TJ), 2) southern Hebei (HB), 3) middle Shanxi (SX) and 4) north central Shandong (SD). Meanwhile, there is a secondary intensive source zone over northern SX. In Fig. 3, overall primary particle source emission intensity decreases to its lowest level at 05:00. Thereafter, emission intensity begins to

180   increase and remains high from 11:00 to 19:00, with a little trough at 14:00. The source intensity temporal profile of every particle species is similar, and sulphate is illustrated for example.

Measurements used in this paper were obtained from the observation stations of Chinese Research Academy of Environmental Sciences (CREAS: 116.39°E, 40.03°N), the Guanyuan (GY: 116.34°E, 39.93°N) and the Dingling (DL: 116.22°E, 40.29°N). The CRAES station locates in northwest Chaoyang District at the Chinese Academy of Environmental

185   Sciences, and the GY station locates at Xicheng district. Both the CREAS station and the GY station are representative urban

observation stations in Beijing. The DL station locates in relatively clean Changping district at northern Beijing and provides background values of observed $PM_{2.5}$ concentrations.

The reliability of the GRAPES-CUACE modelling system is evaluated by comparisons with hourly $PM_{2.5}$ concentration observations from 20:00 LT 17 November to 20:00 LT 22 November at CREAS, GY and DL observational stations (Figs. 5a-c, Table 1). Figure 5a-c show the observed and simulated hourly $PM_{2.5}$ concentration curves from 20:00 LT 17 November to 20:00 LT 22 November, and Table 1 lists the statistical metrics. Figure 5a-c reveal that the results of the GRAPES–CUACE modelling system correspond well with the synoptic analysis of the pollution episode. The modelling system reproduces the $PM_{2.5}$ accumulation processes from 19 to 21 November in Beijing, and captures the two $PM_{2.5}$ hourly concentration peaks during the dawn and night of 21 November, as well as the trough during 21 November afternoon at CREAS, GY and DL stations, with correlation coefficients (Rs) of 0.87, 0.91 and 0.69, respectively (Table 1). However, the model overestimates $PM_{2.5}$ concentration values over the period with normalized mean biases (NMBs) of 57.2%, 108.1% and 10.7% at CREAS, GY and DL stations, respectively. The over-estimation is also reflected by positive mean bias (MB) and mean fractional bias (MFB) values. MFBs at CREAS, GY and DL stations are 53.6%, 65.2% and 15.6%, respectively, whereas corresponding mean fractional errors (MFEs) are correspondingly 60.1%, 68.3% and 39.6%. MFEs and MFBs are all within the criteria proposed by Boylan and Russel (2006) —that is, model performance criteria have been met when MFE and the MFB are less than or equal to approximately +75% and $\pm 60\%$, respectively—except for the MFB at GY, which is a little high. Model overestimation might be attributable to the coarse resolution of the model settings (0.5°×0.5°) and local environmental interference at the observation site. Prior studies (Zhou et. al., 2012; Wang et al., 2015a; Wang et. al., 2015b; Jiang et. al., 2015) have proven the stable simulation performance of the GRAPES–CUACE modelling system in reproducing air pollution levels and variation trends over northeast China. Above all, the following analysis mainly focussed on the variations and contribution proportions of emission sources over different regions, so these modelling results can be considered reliable.

4. Results

4.1. Simulated haze episode and objective function

Figure 6 shows the simulated surface $PM_{2.5}$ concentration and wind field variations from 17:00 LT on 19 November to 11:00 LT on 22 November It can be seen that the simulation results are consistent with the qualitative weather analysis of this time period. From 19 to 20 November, $PM_{2.5}$ accumulated in Beijing under the influence of a convergent wind field pattern: a southerly wind field to the south, an easterly wind field to the east and a westerly wind field to the west. From 5:00 LT to 11:00 LT on 21 November, $PM_{2.5}$ concentrations exceeded 550μg m^{-3} over southern Beijing, south-central Hebei and northwest Tianjin. After this peak, $PM_{2.5}$ concentration over Beijing, south-central Hebei and Tianjin decreased to a trough in the afternoon, before rising again above 550μg m^{-3} at 23:00 LT. The decrease of $PM_{2.5}$ from the morning to the afternoon was

typical for Beijing, and resulted mainly from diurnal variation of the planetary boundary layer, with vertical mixing after sunrise effectively diluting pollutants (Zhao et al., 2009; Liu et al., 2015; Tang et al., 2016). The concentration peak at 23:00 LT was driven by the influence of the easterly winds, which caused pollutant convergence against the Taihang Mountains, and carried abundant water vapour that promoted local hygroscopic growth. Afterwards, during the daytime of 22 November, a notable northwesterly wind dispersed pollutants in Beijing, thus ending this pollution episode.

Beijing municipality (area that cover both rural and urban Beijing) experienced two hourly $PM_{2.5}$ concentration peaks at 5:00 LT and 23:00 LT on 21 November (Figure 5d), similar to those observed at the three observation stations. These peaks resulted in the high daily average $PM_{2.5}$ concentration on 21 November, which was analysed in previous research (Zhai et al., 2016). In order to analyse the critical emission sources of the two hourly $PM_{2.5}$ concentration peaks, we took advantage of the adjoint model in simulating concentration-emission relationships and defined two objective functions as the hourly mean $PM_{2.5}$ concentration over Beijing at (i) 5:00 LT and (ii) 23:00 LT on 21 November. To demonstrate the reliability and efficiency of the GRAPES–CUACE aerosol adjoint model to provide guidance toward effective and flexible air quality control designs, a third objective function was defined as (iii) average $PM_{2.5}$ concentration over Beijing on 21 November. Subsequently, comparisons between results from the GRAPES–CUACE aerosol adjoint model and the Models-3/CMAQ assessments (Zhai et al., 2016) were made.

4.2. Spatial distribution of primary $PM_{2.5}$ emission sources sensitivity coefficients

Figure 7 illustrates the distribution of time-integrated sensitivity coefficients to emission sources for the two concentration peaks in the hourly $PM_{2.5}$ in Beijing. The sensitivity coefficients of the objective function to emission sources connected pollutants with emissions and revealed the incremental impacts of emissions on peak $PM_{2.5}$ concentrations. The larger the sensitivity coefficient value is, the greater its influence on the objective function J. For example, the largest sensitivity coefficient in Figure 7d was in the cell that includes Daxing district, with a value of $22.4 \mu g\ m^{-3}$. This indicates that emissions emitted in this area had the greatest influence on the peak concentration when integrated over 72 hours. If emissions were reduced within a small range, decrease of $PM_{2.5}$ concentration should be linear. For example, if emissions from this cell were reduced by N% from 05:00 LT 18 November to 05:00 LT 21 November, the target $PM_{2.5}$ concentration would decrease by $N\%*22.4 \mu g\ m^{-3}$.

In Figure 7a and 7d and Figure 7e and 7h, with the accumulation along inverse time sequence, the more influential regions (regions with relatively larger sensitivity coefficients) extended from local Beijing (the target region that covers the entire Beijing municipality) to its surrounding provinces. This phenomenon reflects that in this pollution episode, $PM_{2.5}$ in Beijing was not only the result of local emissions, but also the result of emissions from surrounding regions, including Hebei province, Tianjin and even Shanxi and Shandong provinces. Emissions from the surrounding areas were continuously transported to Beijing 2 to 3 days ahead of the peak pollution day, leading to the observed increase in Beijing's air pollutant concentration.

There are differences in the variations of the more sensitive emission regions of these two $PM_{2.5}$ concentration peaks. First, comparing the 12-hour cumulative sensitivity coefficients distribution in Figure 7b and 7f, we can see that emissions to the southwest of Beijing already had a clear influence on the 05:00 LT 21 November $PM_{2.5}$ concentration peak (Figure 7b), however, for the 23:00 LT 21 November $PM_{2.5}$ concentration peak, influential emission sources still concentrate over Beijing municipality (Figure 7f), with only a small fraction of influential emissions coming from east and south of Beijing. This is due to the southwesterly airstream positioned to the southwest of Beijing from 23:00 LT on 20 November to 05:00 LT on 21 November and the southeasterly water vapour import during the afternoon and night of 21 November, which caused moisture–absorption growth of local particles and brought pollutants from Tianjin.

Second, it can be seen from the distributions of the 24-h (Figure 7c and 7g) and 72-h (Figure 7d and 7h) cumulative sensitivity coefficients that sensitivity coefficients both in and around Beijing had relatively large values, which reflects that both of these $PM_{2.5}$ concentration peaks are influenced by local and surrounding emissions. However, the most influential emission regions differed between the two $PM_{2.5}$ concentration peaks. For the first $PM_{2.5}$ concentration peak, the key 24-h source regions (Figure 7c) are distributed over Beijing and the west and south of Beijing and the key 72-h source regions (Figure 7g) are to the northeast, in Shanxi province. However for the second $PM_{2.5}$ concentration peak, the key 24-h source regions are mainly located to the south of Beijing, and the key 72-h source regions are to the west of Beijing (Shanxi province) (Figure 7h), and cover a smaller area than that for the first $PM_{2.5}$ concentration peak (Figure 7d).

The results of these simulations show that the variation of the sensitivity coefficients distribution, the meteorological condition and the pollution evolution processes correspond with each other very well. This indicates that the GRAPES–CUACE aerosol adjoint model is capable of estimating the sensitivity of concentration to emission sources by propagating a perturbation in concentration backward in time with incorporating meteorological and chemical processes.

4.3. Local and surrounding emission sources influence on peak $PM_{2.5}$ concentrations

Figure 8 illustrates the hourly instantaneous sensitivity coefficients to local and surrounding emission sources (Figure 8a and 8b) and their corresponding time-integrated series (Figure 8c and 8d). The magnitudes of the sensitivity coefficients reflect the incremental influence of local and surrounding emissions to the objective $PM_{2.5}$ peaks. It can be seen that the instantaneous sensitivity coefficients of the $PM_{2.5}$ concentration peaks to local (red closed squares) and surrounding (red open squares) emissions ascended to their maximal points before showing a decreasing tendency. However, detailed comparisons of the hourly contribution of local and surrounding emissions revealed their significant differences.

Analysing Figure 8a and 8b along a reversed time sequence, the maximum of the local emission sensitivity coefficients (red closed squares) and the $PM_{2.5}$ concentration peaks (blue closed circles) appeared at almost the same time, with the latter delayed by 1 to 2 hours. This indicates that local emissions released 1 to 2 hours ahead of the $PM_{2.5}$ peak values have the largest influence on the peak pollution concentrations. After the sensitivity coefficient maximum points, local emission sensitivity

coefficients decrease sharply to minimal values at 14 hours (for the 05:00 $PM_{2.5}$ peak) or 19 hours (for the 23:00 $PM_{2.5}$ peak) ahead of the pollution peak and then stay low. This revealed that $PM_{2.5}$ generated from local emissions was transported away from Beijing after about 14–19 hours.

In contrast, maximal sensitivity coefficients of the surrounding emissions (red open squares) occurred 7–12 hours ahead of the $PM_{2.5}$ concentration peaks (Figure 8a and 8b), which indicates a 7- to 12-hour delay for emissions from surrounding areas to arrive to Beijing. As with backward integration, sensitivity coefficients show overall decreasing trends with periodic fluctuations. For the first $PM_{2.5}$ concentration peak (05:00 LT 21 November), three maximal contributions from surrounding areas (Figure 8a) appeared at 17:00 LT 20 November (12 hours ahead of the target time), 1:00 LT 20 November (28 hours ahead of the target time) and 4:00 LT 19 November (49 hours ahead of the target time), respectively, along the reversed time sequence. The first time-reversed relative maximal sensitivity coefficient, at 17:00 LT on 20 November is 7.5μg m^{-3}, while the second and the third time-reversed relative maximal sensitivity coefficients at 1:00 LT on 20 November and 4:00 LT on 19 November are 5.2μg m^{-3} and 1.5μg m^{-3} respectively. For the second $PM_{2.5}$ concentration peak (23:00 LT on 21 November) (Figure 8b), the relative maximal contributions from surrounding areas (red open squares) appear at 16:00 LT on 21 November (7 hours ahead of the objective time), 20:00 LT on 20 November (27 hours ahead of the objective time), 23:00 LT on 19 November (48 hours ahead of the objective time) and 3:00 LT 19 November (68 hours ahead of the objective time), and their corresponding sensitivity coefficients are 5.3μg m^{-3}, 5.4μg m^{-3}, 2.6μg m^{-3} and 0.9μg m^{-3} respectively. It is worth noting that sensitivity coefficients maximal points for the 23:00 $PM_{2.5}$ peak appear at time points around sensitivity coefficients maximal points for the 05:00 $PM_{2.5}$ peak. The sensitivity coefficients around the second maximal contribution, approximately from 17:00 LT on 20 November to 0:00 LT on 21 November, remain at a relatively large value (about 4.7 to 5.4μg m^{-3}), even slightly larger than that of the first maximal sensitivity coefficient. This is because the second $PM_{2.5}$ concentration peak is cumulated on the basis of the first high $PM_{2.5}$ concentration peak, thus emissions from the surrounding areas from the night on 20 November to early in the morning on 21 November also have a large influence on the second $PM_{2.5}$ concentration peak, almost slightly rivalling the influence of the later emissions sensitivity peak.

Based on Figure 8, we can also see that for both $PM_{2.5}$ concentration peaks, the dominant emission source areas shifted from the local to the surroundings over backward time sequence (Figs. 8c and 8d). For the first $PM_{2.5}$ concentration peak (05:00 LT on 21 November) (Figure 8c), the cumulative local emission sensitivity coefficients (red closed squares) were larger than the surrounding emission sensitivity coefficients (red open squares) from 12:00 LT on 20 November to 05:00 LT on 21 November (lasted for 17 hours), which indicates that local emissions dominated during this 17-hour time period. For the second $PM_{2.5}$ concentration peak (23:00 LT on 21 November) (Figure 8d), local emissions dominated from 21:00 LT on 20 November to 23:00 LT on 21 November, which lasted for 26 hours, 9 hours longer than that of the first $PM_{2.5}$ peak pollution. This phenomenon again indicates the tiny effect of emissions transport processes on 21 November, and that the increase of $PM_{2.5}$

concentration on 21 November is mainly due to local generation. This reinforces the importance of emissions from surrounding regions in accumulating the first $PM_{2.5}$ concentration peak.

4.4. Emission sources contributions from different provinces around Beijing to peak $PM_{2.5}$ concentrations

We then divided emission sensitivity coefficients into different provinces over Beijing's surroundings to investigate their influence on the $PM_{2.5}$ peaks over Beijing municipality. Fig. 9 illustrates the hourly instantaneous sensitivity coefficients to emission sources from Beijing municipality (BJ), Hebei province (HB), Tianjin city (TJ), Shanxi province (SX) and Shandong province (SD) (Figs. 9a and 9b), their corresponding time-integrated series (Figs. 9c and 9d) and the overall contribution proportions of emission sources from each province to the $PM_{2.5}$ concentration peaks (Figs. 9e and 9f). As shown in Fig. 9, emission sources impacts from BJ, HB, TJ, SX and SD on BJ $PM_{2.5}$ peaks are quite different in both variation trends and magnitudes.

For the 05:00 of 21 November $PM_{2.5}$ peak, emission sources from HB contribute the most among surrounding provinces, and HB's hourly sensitivity coefficients variation shows consistent periodic fluctuations with that of surrounding emissions. Three maximal points of the HB hourly sensitivity coefficients variation occur at the same time as that of surrounding emission sources. Corresponding sensitivity coefficients are $5.3\mu g\ m^{-3}$, $3.2\mu g\ m^{-3}$ and $0.8\mu g\ m^{-3}$, respectively (Fig. 9a). The largest influential time period of emissions from TJ appeared 13 h ahead of the objective time (at 16:00 20 November), followed by an obvious secondary maximal point that appeared 24 h ahead of the objective time (at 05:00 20 November). Sensitivity coefficients from SX show a small peak (about $0.7\mu g\ m^{-3}$) 9 h ahead of the objective time (at 20:00 20 November), which is caused by a secondary intensive emission zone in northern SX and relatively close to BJ (Fig. 2). As intensive emission sources in SX and SD are far from BJ (Fig. 2), it took 33–36 h for SX and SD emissions to reach BJ.

For the 23:00 November 21 $PM_{2.5}$ peak, it's worth noting that, except for the maximal sensitivity coefficients of HB and TJ at 16:00 21 November (7 h ahead of 23:00 21 November), prior sensitivity coefficient maximal points appeared at the same time as the maximal points of sensitivity coefficients when the 05:00 21 November $PM_{2.5}$ concentration peak was set as the objective function. For example, for both $PM_{2.5}$ concentration peaks, sensitivity coefficients of TJ emission sources reached a maximal point at 16:00 20 November, and SX emission source sensitivity coefficients showed two maximal points at 20:00 20 November and 20:00 19 November in turn. The situations at HB and SD are similar, as even when maximal points do not appear at the exact same time, high value periods are consistent for the two objective functions. The above phenomenon again revealed that the 23:00 21 November $PM_{2.5}$ concentration peak was accumulated on the basis of the 05:00 21 November $PM_{2.5}$ concentration peak, and that if the 05:00 21 November $PM_{2.5}$ concentration peak can be effectively reduced, the $PM_{2.5}$ concentration peak at 23:00 21 November can be reduced accordingly, thus decreasing the overall $PM_{2.5}$ concentration on 21 November. These results also reflected the adjoint model's advantage in detecting temporal-spatial sensitive emission sources in detail.

340   Figs. 9c and 9d show that along the backward time sequence, time-integrated sensitivity coefficients of HB continuously rise after time-integrated sensitivity coefficients of other provinces are prone to remain constant. At around 02:00 to 03:00 20 November, the time-cumulated emissions influence from HB exceeded that from local BJ emissions for both $PM_{2.5}$ peaks, which reflected that emissions from HB play a leading role in pollutant accumulation for the first BJ $PM_{2.5}$ peak, and that local emissions influence dominates between the two $PM_{2.5}$ peaks, that is, during the the daytime of 21 November.

345   The hourly sensitivity coefficients in Figs. 9a and 9b show that emission source impacts from Beijing and each surrounding province decrease to negligible values (close to zero) 72 h ahead of the objective time points. Meanwhile, corresponding time-integrated sensitivity coefficients in Figs. 9c and 9d also stop increasing 72 h prior to the objective time points. Therefore, by integrating sensitivity coefficients 72 hours ahead of the two $PM_{2.5}$ concentration peaks, we can obtain the overall contribution proportions of emission sources from each province to the BJ $PM_{2.5}$ peaks (Figs. 9e and 9f). Among all

350 provinces, HB has the largest impact on the two $PM_{2.5}$ concentration peaks, and the contribution of HB emissions to the first $PM_{2.5}$ concentration peak (43.6%) is greater than to the second $PM_{2.5}$ concentration peak (41.5%). The second largest emission source contributing province is Beijing (31.2%), followed by SX (9.8%), TJ (9.8%) and SD (5.7%) for the 05:00 $PM_{2.5}$ peak, and Beijing (35.7%) followed by SX (8.1%), SD (8.0%) and TJ (6.7%) for the 23:00 $PM_{2.5}$ peak.

    From all the above analysis, we can conclude that joint control of air pollutant sources with Hebei province, Tianjin city,

355 Shandong and Shanxi provinces 2 to 3 days ahead of the first $PM_{2.5}$ concentration peak can effectively reduce $PM_{2.5}$ concentration accumulation due to transported pollutants, thus decreasing the concentrations of the BJ $PM_{2.5}$ peaks.

4.5. Comparisons of the adjoint results with Models-3/CMAQ assessments

    Previous research used a back-trajectory model, FLEXPART, to locate sensitive emission regions of Yanqihu, Beijing in November 2012. The study then used the Models-3/CMAQ modelling system to quantify the effects of emission reduction

360 schemes at different ratios, during different time periods and over different regions on $PM_{2.5}$ concentration reduction on 21 November in Beijing (Zhai et al., 2016). Based on this, we set the average $PM_{2.5}$ concentration over Beijing municipality on 21 November as the objective function and compared the adjoint results with the Models-3/CMAQ assessments. Figure 10 illustrates the time-integrated sensitivity coefficient distributions when the Beijing average $PM_{2.5}$ concentration on 21 November was set as the objective function. The magnitudes of the sensitivity coefficients reflect the incremental influence

365 of emissions to the objective $PM_{2.5}$ concentration. As with previous research (Zhai et al., 2016) that advocated joint control of emissions with surrounding provinces 2 to 3 days ahead of the most polluted day, adjoint time-integrated sensitivity intensified and extended during 48- to 72-h backward time integration.

    In order to assess the adjoint sensitive source zone on decreasing $PM_{2.5}$ concentration over Beijing and to compare the adjoint results with the Models-3/CMAQ assessments, we referred to the research by Zhai et al. (2016) and selected four emission

370 regions: the overall Huabei region (HuaB), the sensitive Huabei region (HuaB-sens), the overall Beijing municipality (BJ) and

the sensitive Beijing region (BJ-sens) (Figure 11). Grid cells with 72-h cumulative sensitivity coefficients larger than $3\mu g\ m^{-3}$ were included in the sensitive emission regions (HuaB-sens and BJ-sens), and grid cells with smaller sensitive values are outside the sensitive emission regions. Therefore, sensitive emission regions have relatively larger impact on the $PM_{2.5}$ peak concentrations than regions outside them. Here the HuaB-sens accounts for 10.2% the area of HuaB and the BJ-sens accounts for 60.0% the area of BJ, which makes them analogous to the regions defined by Zhai et al. (2016). In the work by Zhai et al. (2016), HuaB-sens accounts for 17.6% of the area of HuaB and BJ-sens accounts for 54.2% of the area of BJ. In addition, based on emission magnitudes (Fig. 2), we defined regions with emission intensities larger than $4.1\times10^{-7}g\cdot s^{-1}$ within HuaB as the "Emis-intensive" regions (Fig. 11). The Emis-intensive region has the same area as that of the HuaB-sens.

Table 2 lists the ratios of the time cumulative sensitivity coefficients to peak $PM_{2.5}$ concentration (SC/PC) over the BJ, BJ-sens, HuaB, HuaB-sens, and Emis-intensive regions at 3 different time points: 0 days (d0), 1 day (d1) and 2 days (d2) in advance of the most polluted day. The SC/PC reflects the reduction ratios of peak $PM_{2.5}$ concentration due to absence of emissions over different regions and during different periods, that is, emission source contribution ratios to peak $PM_{2.5}$ concentration. From Table 2, we can see that the adjoint results are highly consistent with the Models-3/CMAQ system results (Zhai et al., 2016). The 21 November $PM_{2.5}$ concentration was an accumulated result from emissions released in the day or two days leading up to the most polluted day, rather than a simple result of emissions on 21 November For all the BJ, BJ-sens, HuaB and HuaB-sens regions, emissions contribution ratios grew from 'd0' to 'd2' ('d0', 'd1' and 'd2' are defined in the caption of Table 2), especially from 'd0' to 'd1'. The contribution ratios of emissions from BJ (and BJ-sens) and HuaB (and HuaB-sens) increased by 6.2% (5.8%) and 31.9% (18.9%), respectively, from 'd0' to 'd1'. Thereafter, the contribution ratios again increased by 0.6% (0.5%) and 9.6% (3.6%), respectively, for emissions over BJ (or BJ-sens) and HuaB (or HuaB-sens) from 'd1' to 'd2'. The above phenomenon also indicates that, with the accumulation of time-reversed integration from 48h to 72h prior to 21 November, emission source contributions from HuaB (or HuaB-sens) to peak $PM_{2.5}$ concentration increases more obviously, while emission source contributions from BJ (or BJ-sens) hardly increase at all. This can be explained by surrounding emissions being continuously transported to Beijing 2 to 3 days ahead of the most polluted day (Zhai et al., 2016). Similarly to the work in Models-3/CMAQ assessments, Table 3 shows comparisons of sensitive emission, full emission, and Emis-intense region source contribution effects and efficiencies to peak $PM_{2.5}$ concentration. In Table 3, S/F(effect) in the BJ-sens column refers to the ratios of sensitivity coefficients over BJ-sens to sensitivity coefficients over BJ, and S/F(effect) in the HuaB-sens (or the Emis-intense) column refers to the ratios of sensitivity coefficients over HuaB-sens (or Emis-intense) to sensitivity coefficients over HuaB. Correspondingly, S/F(efficiency) refers to the ratios of sensitivity coefficients per unit area over BJ-sens (or over HuaB-sens and Emis-intense) to sensitivity coefficients per unit area over BJ (or over HuaB). Therefore, S/F(effect) and S/F(efficiency) reflect emission source reduction effects and reduction efficiency over sensitive (or emission intensive) regions. The implication of 'd0', 'd1' and 'd2' in Table 3 are the same as they are in

Table 2. As shown in Table 3, the contribution efficiencies (contribution ratios per unit area) of emissions from the HuaB-sens and BJ-sens are significantly higher than those from the corresponding entire HuaB and BJ regions respectively. Although BJ-sens covers only 60% the area of the entire BJ, its contribution to the peak $PM_{2.5}$ concentration is 86.6%–88.2% of that of the entire BJ. Its source contribution efficiency is 1.4 to 1.5 times that of BJ. Similarly, HuaB-sens covers only 10.2% the area of the entire HuaB, its contribution to the peak $PM_{2.5}$ concentration is 61.0%–71.9% of that of the entire HuaB, and its source contribution efficiency is 6.0-7.0 times that of the entire HuaB (Table 3). Finally, emissions from HuaB-sens contribute much more than emissions only from BJ-sens, which supports joint control. Analogously, in the Models-3/CMAQ assessments, BJ-sens (or HuaB-sens) covers 54.2% (or 17.6) the area of BJ (or HuaB), and its emissions reduction effect is 99.2%–100% (or 87.2%-93.7%) of that of the entire BJ (or HuaB), and its source contribution efficiency is 1.8 to 1.9 times (or 5.0 to 5.3 times) that of BJ (or HuaB).

We then compared emission source contribution ratios, effect and efficiency from the HuaB-sens and the Emis-intense regions. As shown in Table 2 and Table 3, although the Emis-intense region has the same area as HuaB-sens, its SC/PC, S/F (effect) and S/F(efficiency) are all much smaller. The source contribution ratios to $PM_{2.5}$ concentration on 21 November (SC/PC) from 'Emis-intense' are 9.7%, 17.6% and 18.5% smaller than those from HuaB-sens (Table 2), and the source contribution effect from 'Emis-intense' regions (S/F (effect)) are 37.9%, 30.7% and 27.6% smaller than the S/F (effect) of HuaB-sens, indicating that controlling air pollutant sources from adjoint sensitive emission regions has better effects and higher efficiency than controlling emission sources from emission-intensive regions.

The computational loads of the adjoint simulation were much smaller than the comparable assessments made with the Models-3/CMAQ modelling (Zhai et al., 2016). For the adjoint simulation, one forward integration (for un-equilibrated data saving) and one backward adjoint integration can obtain the influence of emissions from any source region, during any time period to $PM_{2.5}$ peaks. For the Models-3/CMAQ assessments, to compare the effects of emission reductions over two different time periods, at two different ratios and over four different regions, 12 sensitivity tests with a control simulation are required.

5. **Conclusions**

In this research, the GRAPES–CUACE aerosol adjoint model was applied to detect the pivotal emission sources of a November 2012 haze episode, and the hourly peak $PM_{2.5}$ concentrations at 05:00 LT and 23:00 LT on 21 November 2012 over Beijing were set as the objective functions. Contributions to $PM_{2.5}$ concentration peaks from local Beijing and its surrounding provinces were compared. The adjoint results correspond well with the real weather analysis for this period, and correctly describe the spatial distribution of the most influential emission sources over time for both $PM_{2.5}$ concentration peaks. The 05:00 $PM_{2.5}$ concentration peak was mainly influenced by local Beijing emissions, and the emissions from Hebei, Tianjin and Shanxi, due to transmission of pollutants 2 to 3 days ahead of the peak time. The 23:00 $PM_{2.5}$ concentration peak was more

sensitive to local Beijing emissions, and the regions to the south of Beijing, in Hebei province, because of accumulation from the first $PM_{2.5}$ concentration peak and local particle hygroscopic growth and pollutants trapped against of the Taihang Mountains on 21 November. The upstream Hebei province has the largest impacts on both $PM_{2.5}$ concentration peaks, and the contribution of Hebei emissions to the first $PM_{2.5}$ concentration peak (43.6%) is greater than to the second $PM_{2.5}$ concentration peak (41.5%). In Beijing, $PM_{2.5}$ concentration peaks respond to local emissions in 1 to 2 hours, while surrounding emissions take 7 to 12 hours to influence Beijing's air quality.

We compared the adjoint results with Models-3/CMAQ assessments and found that the adjoint results can provide evidence for all the conclusions supported by the Models-3/CMAQ assessments (Zhai et al., 2016). We then defined the 'Emis-intense' region as an emission-intensive region within Huabei region that has the same area of that of sensitive Huabei region (HuaB-sens) and compared its emission source contributions with those of HuaB-sens and Huabei. Overall, we concluded that narrowing emission sources reduction scope to sensitive source zones (zones detected by an adjoint model or a FLEXPART model), rather than emission intensive regions, 2 to 3 days prior to unfavorable meteorological conditions can effectively decrease $PM_{2.5}$ concentration and improve the efficiency of $PM_{2.5}$ reduction measures. Meanwhile, the adjoint simulation is far more computationally efficient than the assessments with Models-3/CMAQ modelling. The adjoint method is a powerful tool for simulating the relationship between emissions and concentrations, and it can be utilised to help improve flexible air quality control schemes.

References:

An, X. Q., Zhai, S. X., Jin, M., Gong, S. L., and Wang, Y.: Development of an adjoint model of GRAPES–CUACE and its application in tracking influential haze source areas in north China, Geosci. Model Dev., 9, 2153-2165, 2016.

An, X. Q., Zhu, T., Wang, Z. F., Li, C. Y., and Wang, Y. S.: A modeling analysis of a heavy air pollution episode occurred in Beijing, Atmos. Chem. Phys., 7(12), 3103-3114, 2007.

Cao, G. L., Zhang, X. Y., Gong, S. L., An, X. Q., Wang, Y. Q.: Emission inventories of primary particles and pollutant gases for China. Chinese Sci Bull, 56, doi:10.1007/s11434-011-4373-7, 2011.

Carmichael, G. R., Sandu, A., Chai, T. F., Daescu, N. D., Constantinescu, E. M., and Tang Y. H.: Predicting air quality: Improvements through advanced methods to integrate models and measurements, Journal of Computational Physics., 227(7): 3540-3571, 2008.

Constantin, B. V. and Barrett, S. R.: Application of the complex step method to chemistry-transport modeling, Atmos. Environ., 99: 457-465, 2014.

Chen, Z. Y., Xu, B., Cai, J., and Gao B. B.: Understanding temporal patterns and characteristics of air quality in Beijing: A local and regional perspective, Atmos. Environ., 127: 303-315, 2016.

Errico, R. M.: What is an adjoint model? Bulletin of the American Meteorological Society, 78(11), 2577-2591, 1997.

Gao, M., Carmichael, G. R., Wang, Y., Saide, P. E., Yu, M., Xin, J., Liu, Z., and Wang, Z.: Modeling study of the 2010 regional haze event in the North China Plain, Atmos. Chem. Phys., 16(3), 1673-1691, 2016.

Guo, Y. M., Tong, S. L., Li, S. S., Barnett, A. G., Yu, W. W., Zhang, Y. S., and Pan, X. C.: Gaseous air pollution and emergency hospital visits for hypertension in Beijing, China: a time-stratified case-crossover study, Environmental Health, 9(1), 57, 2010.

Hakami, A., Henze, D. K., Seinfeld, J. H., Singh, K., Sandu, A., Kim, S., Byun, D. and Li, Q.: The adjoint of CMAQ. Environmental science & technology 41(22): 7807-7817, 2007.

Henze, D. K., Seinfeld, J. H., and Shindell, D. T.: Inverse modeling and mapping US air quality influences of inorganic PM 2.5 precursor emissions using the adjoint of GEOS-Chem, Atmos. Chem. and Phys., 9(16) ,5877-5903, 2009.

Jiang, C., Wang H., Zhao T. L., Li T., and Che H.: Modeling study of $PM_{2.5}$ pollutant transport across cities in China's Jing-Jin-Ji region during a severe haze episode in December 2013, Atmos. Chem. Phys., 15(10), 5803-5814, 2015.

Li, L. J., Wang, Z. S., Zhang, D. W., Chen, T., Jiang, L., and Li, Y. T.: Analysis of heavy air pollution episodes in Beijing during 2013-2014, China Environmental Science, 36(1): 27-35, 2016 (in Chinese).

Liu, Z., Hu, B., Wang, L., Wu, F., Gao, W., and Wang, Y.: Seasonal and diurnal variation in particulate matter (PM_{10} and $PM_{2.5}$) at an urban site of Beijing: analyses from a 9-year study, Environmental Science and Pollution Research, 22, 627-642, 2015.

Marchuk, G.: Numerical solution of the problems of the dynamics of the atmosphere and the ocean (In Russian), Gidrometeoizdat, 1974.

Sandu, A., Daescu, D. N., Carmichael, G. R., and Chai, T.: Adjoint sensitivity analysis of regional air quality models, Journal of Computational Physics, 204, 222-252, 2005.

Sun, Y. L., Jiang, Q., Wang, Z., Fu, P. Q., Li, J., Yang T., and Yin, Y.: Investigation of the sources and evolution processes of severe haze pollution in Beijing in January 2013, Journal of Geophysical Research: Atmospheres, 119(7), 4380-4398, 2014.

Stockwell, W. R., Middleton, P., Change, J. S. and Tang, X.: The second generation regional acid deposition model chemical mechanism for regional air quality modeling. J. Geophys. Res. 95, 16343_16376, 1990.

Tang, G., Zhang, J., Zhu, X., Song, T., Münkel, C., Hu, B., Schäfer, K., Liu, Z., Zhang, J., Wang, L., Xin, J., Suppan, P. and Wang, Y.: Mixing layer height and its implications for air pollution over Beijing, China. Atmos. Chem. Phys. 16(4): 2459-2475, 2016.

Wang, H., Shi, G. Y., Zhang, X. Y., Gong, S. L., Tan, S. C., Chen, B., Che, H. Z., and Li, T.: Mesoscale modelling study of the interactions between aerosols and PBL meteorology during a haze episode in China Jing-Jin-Ji and its near surrounding region – Part 2: Aerosols' radiative feedback effects, Atmos. Chem. Phys., 15, 3277-3287, 2015a.

Wang, H., Xue, M., Zhang, X. Y., Liu, H. L., Zhou, C. H., Tan, S. C., Che, H. Z., Chen, B., and Li, T.: Mesoscale modelling

study of the interactions between aerosols and PBL meteorology during a haze episode in Jing-Jin-Ji (China) and its nearby

495   surrounding region – Part 1: Aerosol distributions and meteorological features, Atmos. Chem. Phys., 15, 3257-3275, 2015b.

Wang, L. T., Wei, Z., Wei, W., Fu, J. S., Meng, C. C., and Ma, S.: Source apportionment of $PM_{2.5}$ in top polluted cities in

Hebei, China using the CMAQ model, Atmos. Environ., 122, 723-736, 2015.

Wu, D., Xu, Y., and Zhang S. Q.: Will joint regional air pollution control be more cost-effective? An empirical study of

China's Beijing–Tianjin–Hebei region, Journal of Environmental Management, 149, 27-36, 2015.

500   Xue, J. and Chen, D.: Scientific Design and Application of Numerical Predicting System GRAPES, Science Press, Beijing,

2008.

Zhai, S. X., An, X. Q., Liu, Z., Sun, Z. B., and Hou, Q.: Model assessment of atmospheric pollution control schemes for

critical emission regions, Atmos. Environ., 124, Part B, 367-377, 2016.

Zhang, H. F., Wang, S. X., Hao, J. M., Wang, X. M., Wang, S. L., Chai, F. H., and Li, M.: Air pollution and control action in

505   Beijing, Journal of Cleaner Production, 112, Part 2: 1519-1527, 2016.

Zhang, L., Liu, L. C., Zhao, Y. H., Gong, S. L., Zhang, X. Y., Henze, D. K., Capps, S. L., Fu, T. M., Zhang, Q., and Wang, Y.

X.: Source attribution of particulate matter pollution over North China with the adjoint method, Environmental Research

Letters 10(8): 084011, 2015.

Zhou C. H., Gong S. L., Zhang X. Y., Liu H. L., Xue M., Cao G. L., An X. Q., Che H. Z., Zhang Y. M., and Niu T.: Towards

510   the improvements of simulating the chemical and optical properties of Chinese aerosols using an online coupled model –

CUACE/Aero, Tellus B, 64(0), 2012.

Table 1 Performance statistics of PM$_{2.5}$ concentration.

Simulated Time Period	Stations	Obs. (µg·m^{-3})	Sim. (µg·m^{-3})	R	MB (µg·m^{-3})	NMB (%)	NME (%)	MFB (%)	MFE (%)
20:00 Nov. 17-22, 2012	CREAS	121.5	190.9	0.87	69.4	57.2	185.2	53.6	60.1
	GY	139.0	289.4	0.91	150.4	108.1	183.3	65.2	68.3
	DL	101.4	112.2	0.69	10.8	10.7	85.6	15.6	39.6

Notes: Mean bias: $MB = \frac{1}{n}\sum_{i=1}^{n}(Sim_i - Obs_i)$;

Normalized mean bias: $NMB = \frac{\sum_{i=1}^{N}(Sim_i - Obs_i)}{\sum_{i=1}^{N} Obs_i} \times 100\%$; Normal mean error: $NME = \frac{1}{n}\sum_{i=1}^{n}\frac{|Sim_i - Obs_i|}{Obs_i} \times 100\%$;

Mean fractional bias: $MFB = \frac{1}{N}\sum_{i=1}^{N}\frac{(Sim_i - Obs_i)}{(Obs_i + Sim_i/2)}$; Mean fractional error: $MFE = \frac{1}{N}\sum_{i=1}^{N}\frac{|Sim_i - Obs_i|}{(Obs_i + Sim_i/2)}$

Table 2 Emission sources contribution to the average PM$_{2.5}$ concentration over Beijing on Nov 21st.

Factors	Time period	BJ	BJ-sens	HuaB	HuaB-sens	Emis-intense
SC/PC	d0	14.5%	12.5%	25.6%	18.4%	8.7%
	d1	20.7%	18.3%	57.5%	37.3%	19.7%
	d2	21.3%	18.8%	67.1%	40.9%	22.4%

Notes: d0 refers to emissions contribution from 21 November; d1 refers to emissions contribution from 20 to 21 November; d2 refers to emissions contribution from 19 to 21 November

SC/PC='time cumulative Sensitivity Coefficient'/'Peak Concentration';

Table 3 Contrast of sensitive (or emis-intense) and full regions emission sources contribution

		GRAPES–CUACE aerosol adjoint model results			Models-3/CMAQ results (Zhai et al., 2016)	
Time period	Factors	BJ-sens	HuaB-sens	Emis-intense	BJ-sens	HuaB-sens
d0	S/F(effect)	86.6%	71.9%	34.0%		
	S/F(efficiency)	1.4	7.0	3.3		
d1	S/F(effect)	88.2%	64.9%	34.2%	99.2%	93.7%
	S/F(efficiency)	1.5	6.3	3.3	1.8	5.3
d2	S/F(effect)	88.2%	61.0%	33.4%	100.8%	87.2%
	S/F(efficiency)	1.5	6.0	3.3	1.9	5.0

Notes: S/F(effect) = 'Sensitivity Coefficient over sensitive source region'/'Sensitivity Coefficient over corresponding full source region';

Contribution Efficiency= 'Sensitivity Coefficient'/'Number of region's simulation grid cells';

S/F(efficiency)= 'Contribution Efficiency of sensitive region'/'Contribution Efficiency of corresponding full source region'.
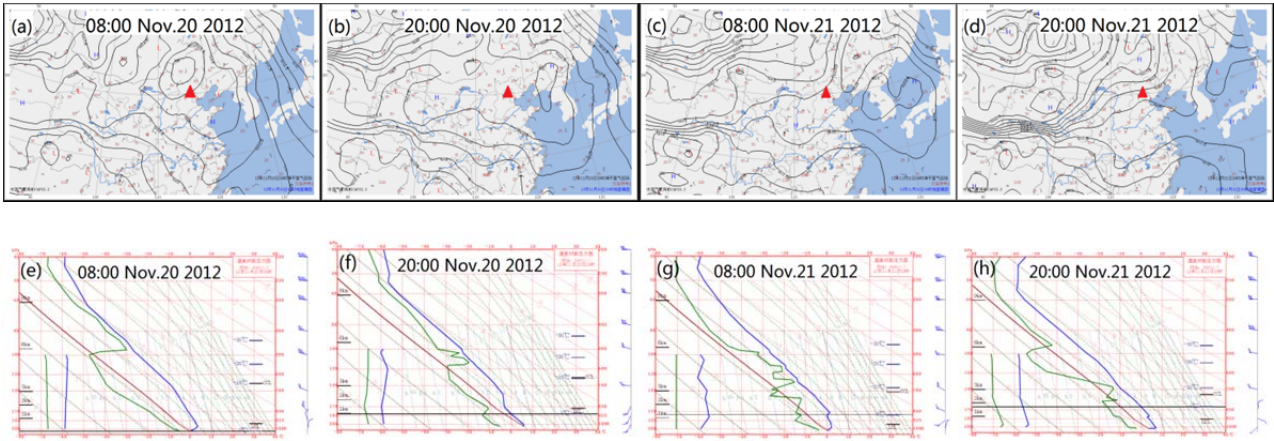
Figure 1. (a–d): Sea-level pressure field (black contour lines; Beijing is marked with red triangle); (e–h): temperature-logarithmic pressure diagrams (thick red solid curves indicate process; green solid curves indicate dew point-pressure; blue solid curves indicate stratification) at Nanjiao Station from 08:00 (local time) on 20 November 2012 to 20:00 (local time) on 21 November 2012. Detailed information in Fig. S1.
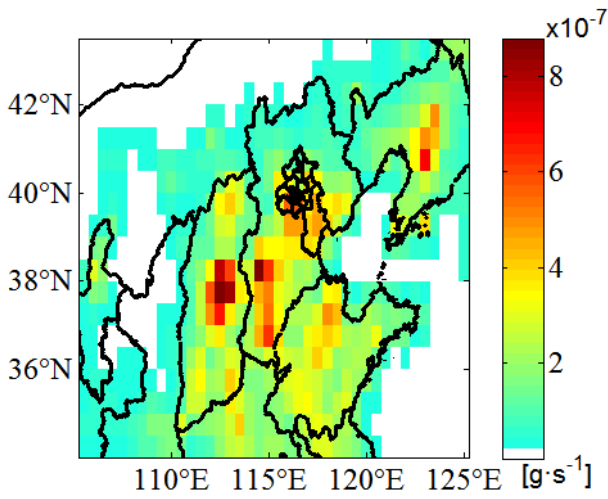
Figure 2. Gridded distribution of PM$_{2.5}$ primary emission sources.
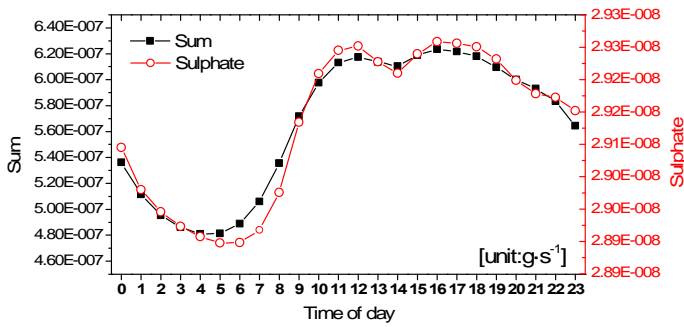
Figure 3. Hourly variation of primary PM$_{2.5}$ emission sources in Beijing.
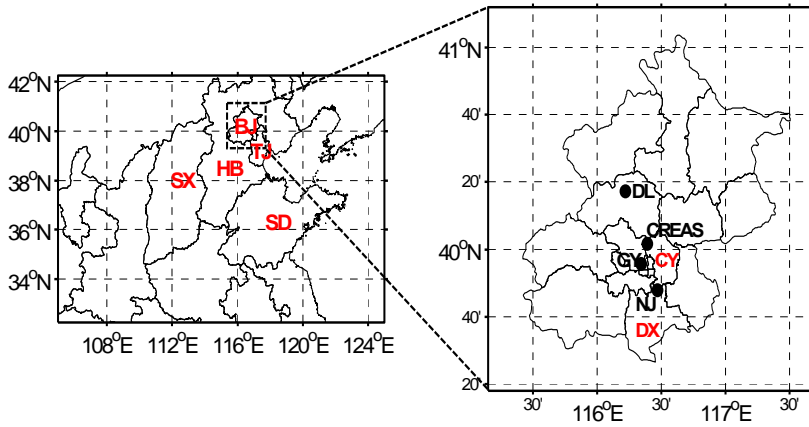
540

Figure 4. Left: Model domain and location of Beijing municipality (BJ), Tianjin municipality (TJ), Heibei province (HB), Shandong province (SD) and Shanxi province (SX); right: Locations of the Chinese Research Academy of Environmental Sciences (CREAS) station, the Guanyuan (GY) station, the Dingling (DL) station, the Nanjiao (NJ) station, Daxing district (DX) and Chaoyang (CY) district.
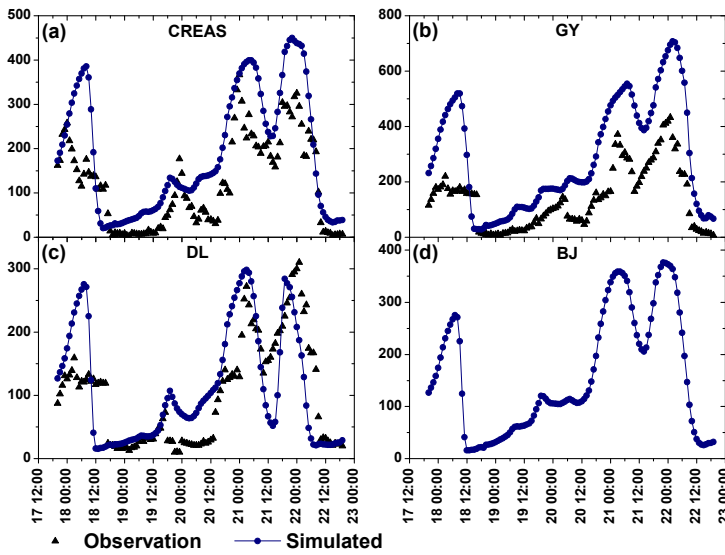
545

Figure 5. (a)-(c): Comparisons of the observed (black solid triangles) and simulated (blue dot-line) hourly PM$_{2.5}$ concentrations at CREAS station, GY station and DL station; (d): Hourly variations of average PM$_{2.5}$ concentration over Beijing municipality.
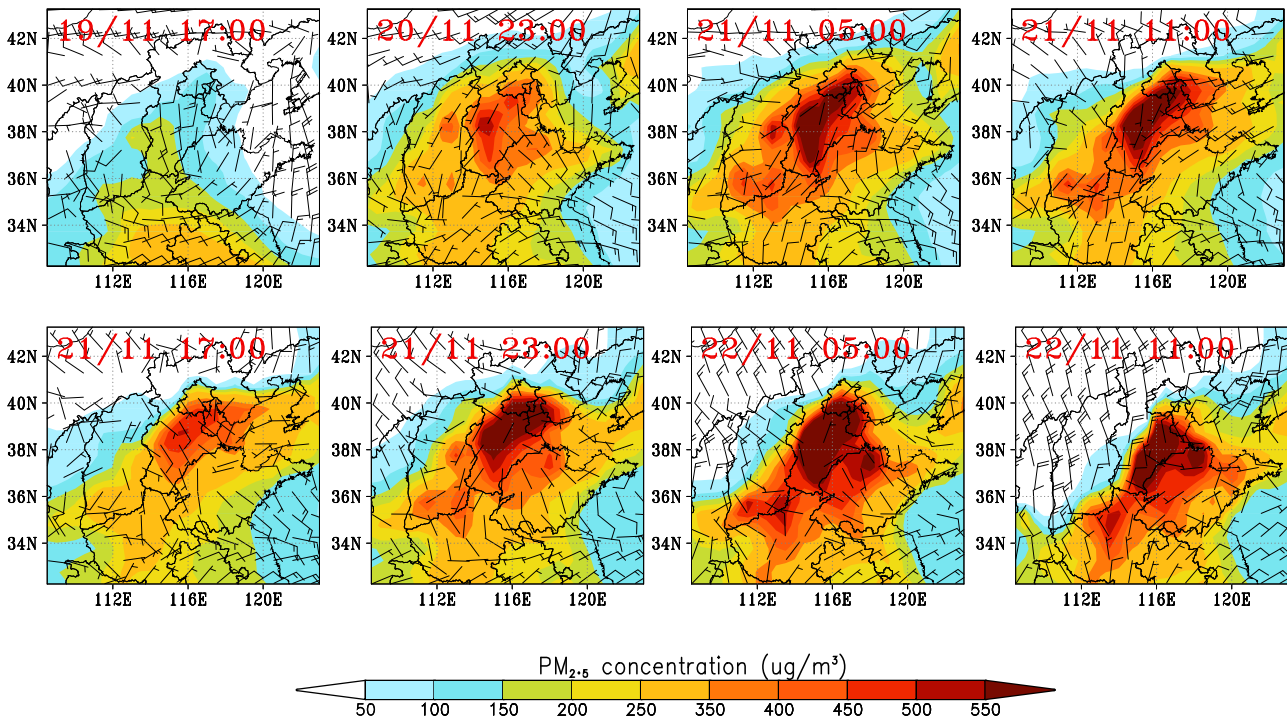
Figure 6. Variations of simulated surface PM₂.₅ concentration and wind field distributions.
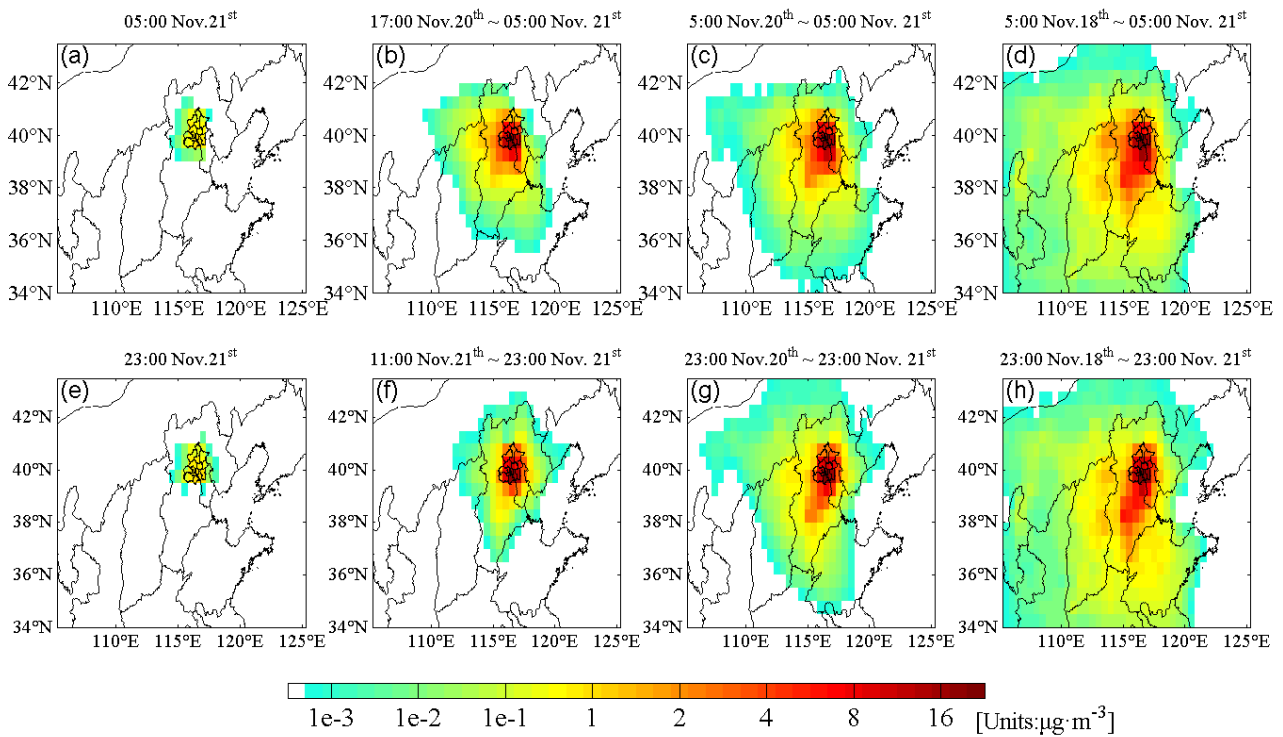
Figure 7. Time-integrated sensitivity coefficients of surface Beijing PM₂.₅ concentration peaks to primary emission sources. (a–d):
1-h, 12-h, 24-h and 72-h integrated sensitivity coefficients for the 5:00 LT on 21 November PM₂.₅ concentration peak; (e–h): 1-h,
12-h, 24-h and 72-h integrated sensitivity coefficients for the 23:00 LT on 21 November PM₂.₅ concentration peak.
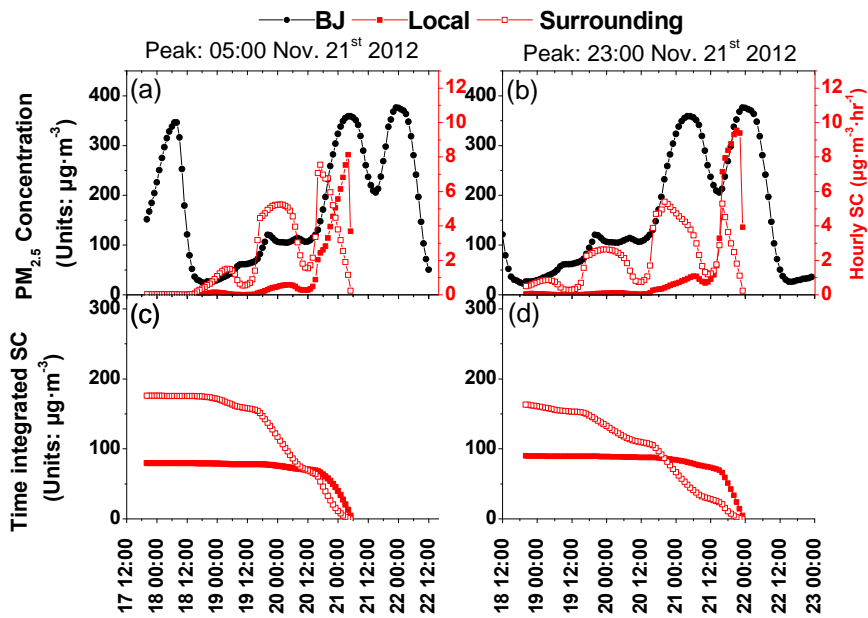
Figure 8. Hourly variations of surface PM$_{2.5}$ concentrations in Beijing and sensitivity coefficients of surface PM$_{2.5}$ concentration peaks in Beijing to local and surrounding primary emission sources. The left and right panels correspond to PM$_{2.5}$ concentration peaks at 05:00 LT and at 23:00 LT on 21 November 2012 respectively. (a–b) illustrate hourly variations of Beijing PM$_{2.5}$ concentration (black solid dot-line) and hourly instantaneously sensitivity coefficients to local (red closed squares) and surrounding (red open squares) emission sources. (c–d) show the time-integrated sensitivity coefficients to local (red closed squares) and surrounding (red open squares) emission sources.
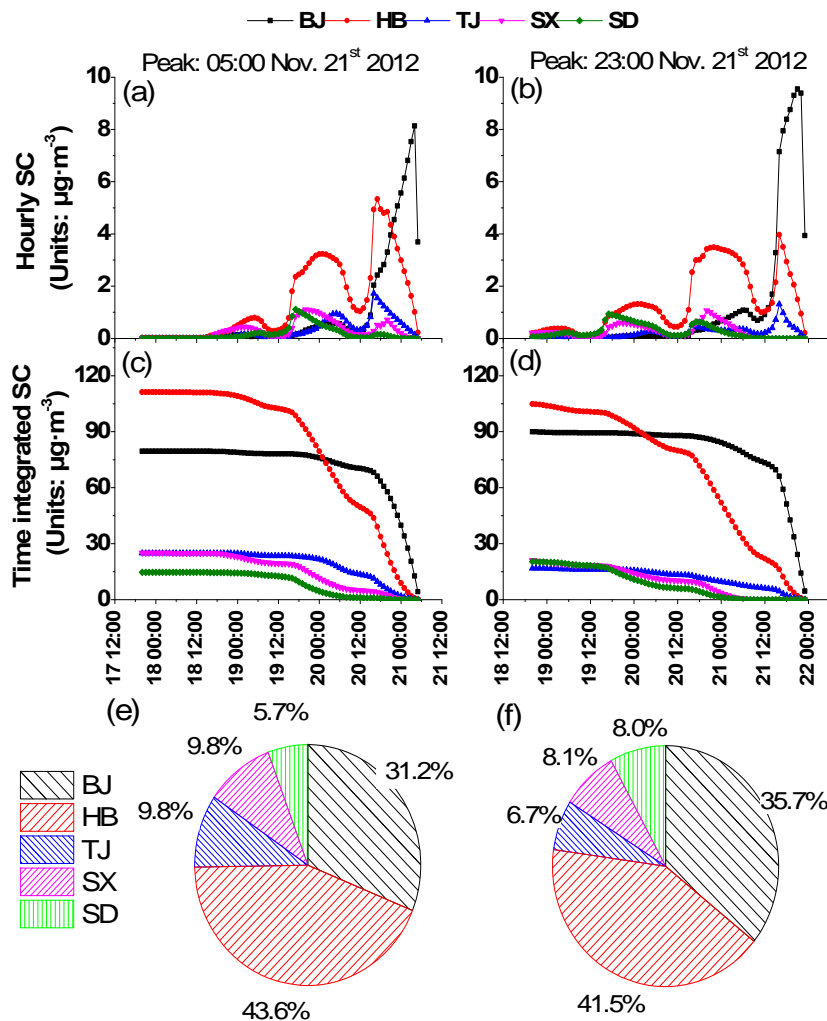
Figure 9. Sensitivity coefficients of surface PM$_{2.5}$ concentration peaks in Beijing to primary emission sources from local Beijing and each of the surrounding provinces. The left and right panels correspond to PM$_{2.5}$ concentration peaks at 05:00 LT and at 23:00 LT on 21 November 2012 respectively. (a–b) illustrate hourly instantaneous sensitivity coefficients to emission sources from local Beijing, Hebei province, Tianjin city, Shanxi province and Shandong province. (c–d) show the time-integrated sensitivity coefficients to local and surrounding provincial emission sources. (e–f) are the contribution ratios of emission sources from each surrounding province to PM$_{2.5}$ concentration peaks.
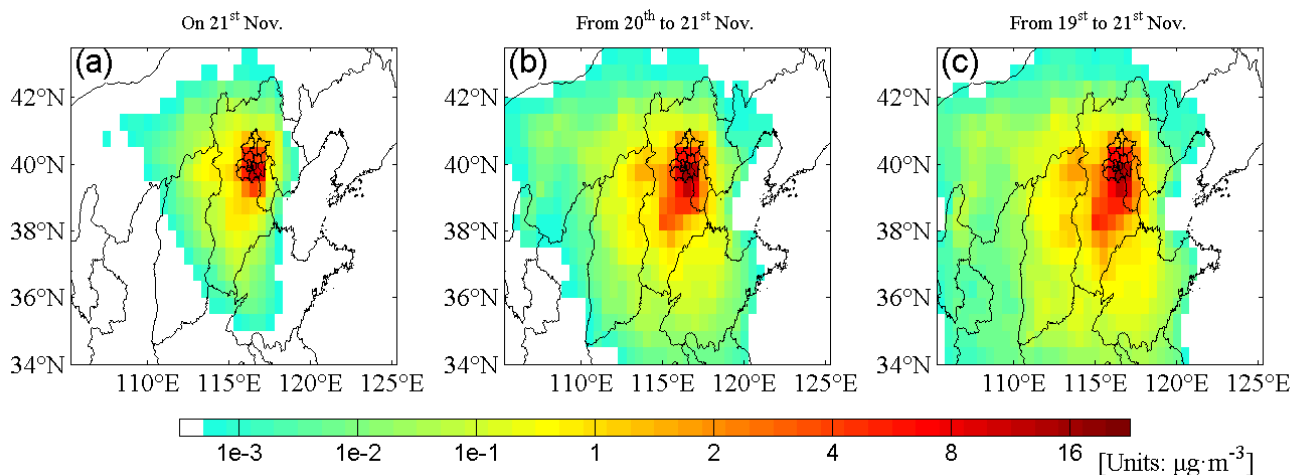
Figure 10. 24-h (a), 48-h (b) and 72-h (c) integrated sensitivity coefficients of surface PM$_{2.5}$ concentrations to primary emission sources in Beijing on 21 November 2012.
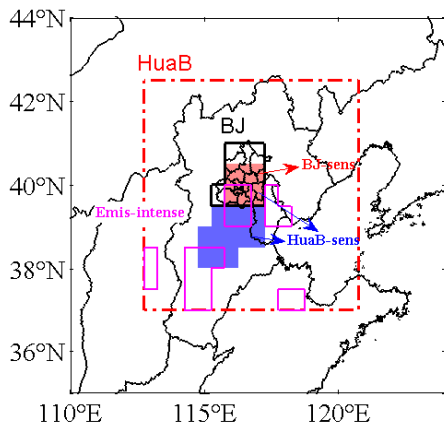
Regions	Number of grid cells	Sensitive area ratios (%)
HuaB-sens	18	10.2
HuaB	176	
BJ-sens	6	60.0
BJ	10	
Emis-intense	18	10.2

Figure 11. Domain definition of Huabei (HuaB, in red dot-dashed frame), Beijing (BJ, in black solid frame), sensitive Beijing (BJ-sens, red shaded), sensitive Huabei (HuaB-sens, red shaded and blue shaded) and emission intensive (Emis-intense, in pink solid frame) regions.

Notes: HuaB-sens area ratio = 'HuaB-sens floor space'/'HuaB floor space'×100%;

BJ-sens area ratio = 'BJ-sens floor space'/'BJ floor space'×100%;

Emis-intense area ratio = 'Emis-intense floor space'/'HuaB floor space'×100%.